Plasmonic Copper Sulfide Nanocrystals Exhibiting Near-Infrared Photothermal and Photodynamic Therapeutic Effects

Shunhao Wang,[†,§,#] Andreas Riedinger,[‡,⊥,#] Hongbo Li,[⊥] Changhui Fu,[†] Huiyu Liu,[*,†] Linlin Li,[†] Tianlong Liu,[†] Longfei Tan,[†] Markus J. Barthel,[⊥] Giammarino Pugliese,[⊥] Francesco De Donato,[⊥] Marco Scotto D'Abbusco,[⊥] Xianwei Meng,[†] Liberato Manna,[⊥] Huan Meng,[*,∥] and Teresa Pellegrino[*,⊥]

[†]Laboratory of Controllable Preparation and Application of Nanomaterials, Research Center for Micro & Nano Materials and Technology, Technical Institute of Physics and Chemistry, Chinese Academy of Sciences, Beijing 100190, People's Republic of China, [‡]Optical Materials Engineering Laboratory, ETH Zurich, 8092 Zurich, Switzerland, [§]University of Chinese Academy of Sciences, Beijing 100049, People's Republic of China, [⊥]Istituto Italiano di Tecnologia, Via Morego 30, 16163 Genova, Italy, and [∥]Division of NanoMedicine, Department of Medicine, University of California, Los Angeles, California 90095, United States. [#]These authors have contributed equally.

ABSTRACT Recently, plasmonic copper sulfide ($Cu_{2-x}S$) nanocrystals (NCs) have attracted much attention as materials for photothermal therapy (PTT). Previous reports have correlated photoinduced cell death to the photothermal heat mechanism of these NCs, and no evidence of their photodynamic properties has been reported yet. Herein we have prepared physiologically stable near-infrared (NIR) plasmonic copper sulfide NCs and analyzed their photothermal and photodynamic properties, including therapeutic potential in cultured melanoma cells and a murine melanoma model. Interestingly, we observe that, besides a high PTT efficacy, these copper sulfide NCs additionally possess intrinsic NIR induced photodynamic activity, whereupon they generate high levels of reactive oxygen species. Furthermore, *in vitro* and *in vivo* acute toxic responses of copper sulfide NCs were also elicited. This study highlights a mechanism of NIR light induced cancer therapy, which could pave the way toward more effective nanotherapeutics.

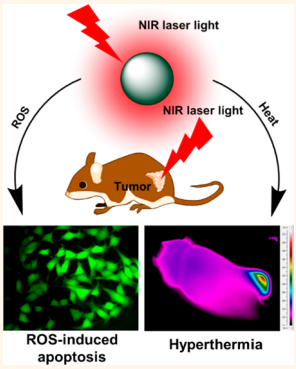

KEYWORDS: copper sulfide nanocrystals · near-infrared light · photothermal therapy · photodynamic therapy

Photodynamic therapy (PDT) refers to phototherapy and photochemotherapy in which photosensitizers (PSs) are used to generate highly reactive oxygen species (ROS) by means of photoexcitation, such as hydroxyl radicals (·OH), singlet oxygen ($^1O_2$), as well as peroxides (R−O−O·) which irreversibly damage a target of interest, for example, cancer cells.[1,2] In clinical applications, the excitation of an ideal PS should occur at a wavelength at which the PS alone and not the tissue absorbs the photon energy.[3] Here, the NIR range of the spectrum (700−1100 nm) is of particular interest since the human tissue is considered to be "transparent" to photons in this energy level.[3] Although many PSs are used in clinics to treat a variety of diseases, PDT in cancer therapy is still hampered by numerous limitations. Organic or metal−organic dyes often have poor water solubility[4] and undergo rapid decomposition under laser irradiation.[5] Other limiting factors include low targeted accumulation[6] and inefficient excitation in the NIR due to low absorption cross sections and/or low extinction coefficients at these wavelengths.[7] In this regard, nanoparticle-based systems represent a potentially useful solution to significantly improve the performance in PDT, with the possibility to overcome all these limitations at once.[6,8,9]

Another novel cancer treatment is represented by photothermal therapy (PTT). Here a therapeutic agent absorbs energy from photons and dissipates it partially in the form of heat. When the therapeutic agent is located in close vicinity[10] to the tumor site, the temperature increase can lead to tumor cell death *via* cellular structure disruption, apoptosis, and/or necrosis mediated mechanisms. Research on PTT has made a huge progress thanks to various NIR light absorbing (plasmonic) nanomaterials that have been developed in the past years. Especially noble metal nanostructures,

* Address correspondence to liuhy@mail.ipc.ac.cn, hmeng@mednet.ucla.edu, teresa.pellegrino@iit.it.

Received for review November 24, 2014 and accepted January 20, 2015.

Published online January 20, 2015
10.1021/nn506687t

such as gold nanospheres,[11] gold nanorods,[12] and gold nanocages,[13] as well as the multifunctional gold nanoshells,[14−16] have been studied intensively in this respect. Lately, cancer therapy by dual PDT and PTT has become the subject of research interest. For example, Liu *et al.* demonstrated an enhanced cellular uptake and cancer cell destruction by a synergistic effect of PEGylated nanographene (as PTT agent) and Chlorin e6 (Ce6) used as PS agent.[17] Choi *et al.* reported that combining gold nanorods (for PTT) with Al(III) phthalocyanine chloride tetrasulfonic acid (AlPcS4) (for PDT) results in significantly enhanced anticancer therapeutic effects.[18] Li *et al.* constructed an assembly of lipid-Hypocrellin B-gold nanocages which allows for synergistic combination of PTT and PDT for cancer therapy working in the NIR region.[19] Nie *et al.* proposed a plasmonic coupling effect between Ce6, the PDT agent, and gold vesicles, the PTT agent.[20] These materials also possessed properties suitable for fluorescence, photoacoustic and thermal imaging.[21] Although considerable efforts have been undertaken in this direction, cancer therapy based on a combination of PDT and PTT is still a challenging task, particularly in an *in vivo* setting. Here we report the working principle of colloidal, NIR plasmonic copper sulfide nanocrystals (NCs) exploitable for both PDT and PTT therapy with NIR activation. Importantly, a key advantage is that through the engineering design, the desired functionalities can be achieved by the intrinsic properties of a single, 6.5 nm in size, crystalline entity, represented by a copper sulfide NC.

In the present work, we focus on copper sulfide NCs of the type $Cu_{2-x}S$, which fall in the class of degenerately doped semiconductors, an emerging new type of NIR plasmonic colloidal NCs.[21−27] Copper chalcogenide NCs are relatively easy to synthesize in both laboratory and larger scales[21,28−30] and are composed of lower cost elements compared to noble metal based NCs. All this makes them promising candidates for low cost and translationable phototherapeutic agents. It has been shown by us and by others that their localized surface plasmon resonance (LSPR) can be tuned by redox reactions through the NIR.[26,31] That allows for modulating their optical properties through their chemical composition.[31,32] Recently, copper chalcogenide ($Cu_{2-x}E$, with E = S, Se, Te) NCs for PTT have been reported by several groups,[33−35] even as heterostructures in combination with noble metal domains.[36] In almost all cases, the functional mechanisms behind the therapeutic effect under NIR irradiation was interpreted as basically due to PTT alone, and other possible concomitant mechanisms were not taken into consideration.

Here we demonstrate that copper sulfide NCs generate elevated ROS levels under NIR laser light irradiation, which results in the parallel therapeutic pathway for PDT. To this end, we synthesized copper sulfide NCs (as described recently by us in in a previous work[30]) and induced oxidation by exposing the NCs to air during the ligand exchange process (from oleylamine to thiolated PEG), by which the formerly hydrophobic NCs were transferred to the aqueous phase. This procedure allowed us to tune the LSPR energy of copper sulfide NCs in the NIR region. Attractively, we show here that, under NIR light irradiation, the leakage of copper ions from copper sulfide NCs can enhance the ROS generation. This effect is highly specific as it occurs only upon irradiation and scales with the reached temperature. Therefore, under a NIR light exposure a combined action of PDT and PTT in Cu-deficient copper sulfide NC was first revealed here. Most importantly, a considerable fraction of their LSPR band is spectrally tunable in the NIR "water window" region, where the light can penetrate deep into the tissues with the negligible ability of heating effect to normal tissue.[37] Also, the light-to-heat conversion efficiency and maximum tolerated dose (MTD) for $Cu_{2-x}S$ NCs were evaluated. The NCs can convert light into heat and enhance ROS generation simultaneously under NIR light irradiation, with a relative high light-to-heat conversion efficiency and acceptable biocompatibility. *In vitro* and *in vivo* results have confirmed the dual action of PDT and PTT elicited by the $Cu_{2-x}S$ NCs, both triggered by NIR laser light.

RESULTS AND DISCUSSION

Copper sulfide NCs ($Cu_{2-x}S$) were prepared by a noninjection approach (Figure 1a).[30] The as-synthesized copper sulfide NCs are capped by oleylamine and can be dispersed in nonpolar organic solvents, such as toluene and chloroform. Figure 1a shows the TEM images of as synthesized $Cu_{2-x}S$ NCs. The average core diameter is 6.5 ± 0.4 nm and the XRD pattern indicates that the main phase is chalcocite, even though also djurleite can be observed (Figure 1b).[38] The chemical composition of the as-synthesized NCs was assessed by inductively coupled atomic emission spectroscopy (ICP-AES), by which a Cu/S ratio equal to 1.88 was determined. Their extinction spectrum before water transfer displays a broad band peaked at around 1800 nm (see Figure 1d), which is attributed to the LSPR for copper deficient copper sulfide NCs. This is in agreement with most of the reported values for copper sulfide NCs with approximate Cu/S ratio of 1.8.[29,33] Oleylamine is a ligand of relatively weak binding affinity, which can be replaced by various other ligands, especially those containing thiol groups.[30] We exploited this to transfer the NCs to aqueous solutions by exchanging the original oleylamine ligands with amphiphilic thiolated PEG molecules (carboxyl-PEG-SH, molecular weight of 3 kDa, and methoxy-PEG-SH, 2 kDa). The PEGylated NCs can be dispersed in polar solvents, including water and other physiological buffers, *e.g.*, phosphate buffered saline solutions (PBS, pH 7.4), and show good

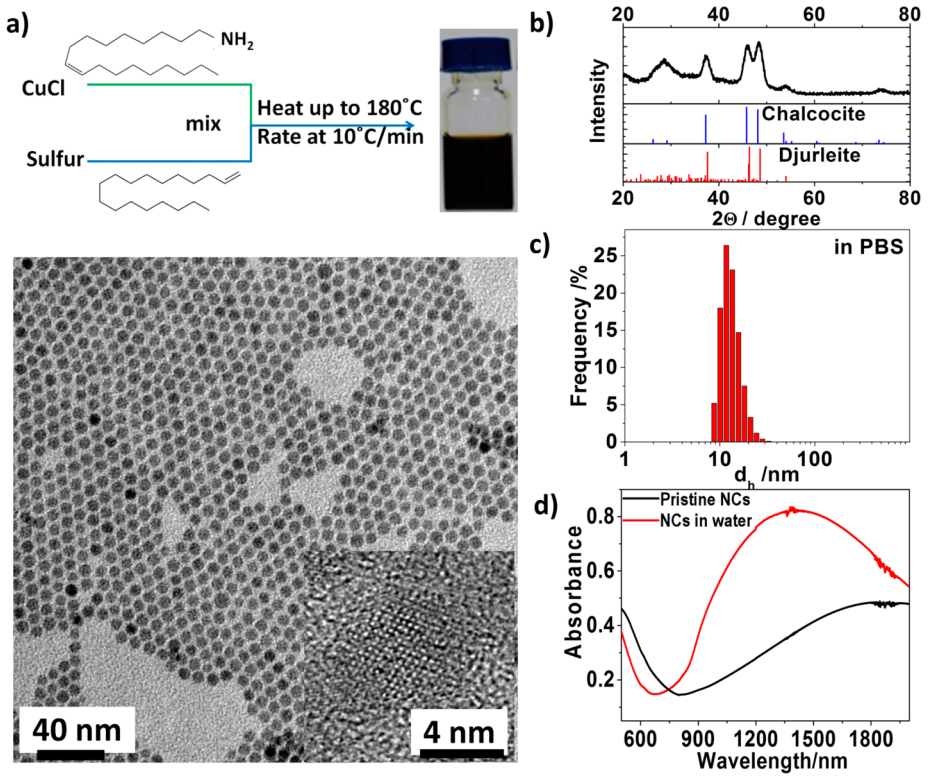

Figure 1. (a) Reaction scheme for the synthesis of $Cu_{2-x}S$ NCs (top) and representative TEM image of the $Cu_{2-x}S$ NCs (bottom). The bottom right inset displays a high resolution TEM image of a single NC. The average diameter of the NCs is 6.5 ± 0.4 nm. (b) XRD pattern of the $Cu_{2-x}S$ NCs, along with bulk patterns for Chalcocite High (PDF Card No. 01-084-0206) and Djurleite (PDF Card No. 00-034-0660). (c) Hydrodynamic diameter distribution of the $Cu_{2-x}S$ NCs in PBS, as assessed by dynamic light scattering (DLS) at 25 °C. (d) Optical absorbance of the pristine $Cu_{2-x}S$ NCs in toluene (black curve) and after ligand exchange and water transfer (red curve). The LSPR band is blue-shifted and narrowed and its intensity is enhanced upon ligand exchange (which is carried out under air), as the NCs are partially oxidized. Oxidation results in an increase of the carrier density in the NCs.

colloidal stability at temperatures below 60 °C. Their hydrodynamic diameters are approximately 12 nm (Figure 1c). The detailed protocol for ligand exchange and water transfer is reported in the experimental section. After the ligand exchange reaction, the Cu/S ratio was close to 1.25, and the LSPR band blue shifted, narrowed, and its intensity increased (see Figure 1d). While a considerable fraction of the sulfur content in the ligand exchanged NCs derives from the thiol groups of the PEG surfactants, the exposure to air leads to partial oxidation of the anion sublattice ($S^{2-} \rightarrow S^{1-} + e^-$) and a fraction of the Cu(I) ions leaves the cation sublattice to establish charge neutrality in each NC.[26] This oxidation introduces additional holes in the upper edge of the valence band and consequently a shift in the LSPR to higher energies due to an increase of the free carrier density (Figure 1d).[24,26,31]

To evaluate the photothermal conversion, $Cu_{2-x}S$ NCs dissolved in PBS at different concentrations were irradiated with a continuous wave (CW) laser at 808 nm with a power density of 2.3 W cm^{-2} (spot size 0.4 cm in diameter) for 10 min and the temperature was recorded online (Supporting Information Figure S1a). Significant heating of the solution was observed, especially at high NC concentrations. At 200 μg mL^{-1} in Cu, the temperature of the solution increased by 30.6 °C in 10 min, while that of pure PBS increased only by 4.13 °C (Supporting Information Figure S1a). By repeating laser on−off cycles, we could raise the temperature at each step without compromising the photothermal efficiency significantly (Supporting Information Figure S1b). Following a previously reported procedure, we could quantify the photothermal efficiency of our NCs to be 16.3% by a NIR laser light heat−cool cycle (the details are reported in Supporting Information Figure S2).[34,39] This value is slightly higher than that of gold nanoshells (13%),[34] but lower than that of recently reported Cu_9S_5 NCs (25.7%)[32] and gold nanorods (21%).[34] However, those nanoparticles (both the Cu_9S_5 NCs and the gold nanorods) were significantly larger in size than our NCs (in both cases they were bigger than 10 nm), thus they had much larger absorption cross sections. One additional advantage of NCs with a realtively smaller size is the ability of nanoparticle extravasation from the fenestration and the ease of intratumoral distribution at the tumor site.[40]

The PEG-coated NCs were found to be colloidally stable up to 60 °C in PBS, while at higher temperatures the NCs started precipitating (see Supporting Information Figure S3). The precipitation occurred both when the sample was exposed to a temperature higher than 60 °C (by incubation) and when it was irradiated with

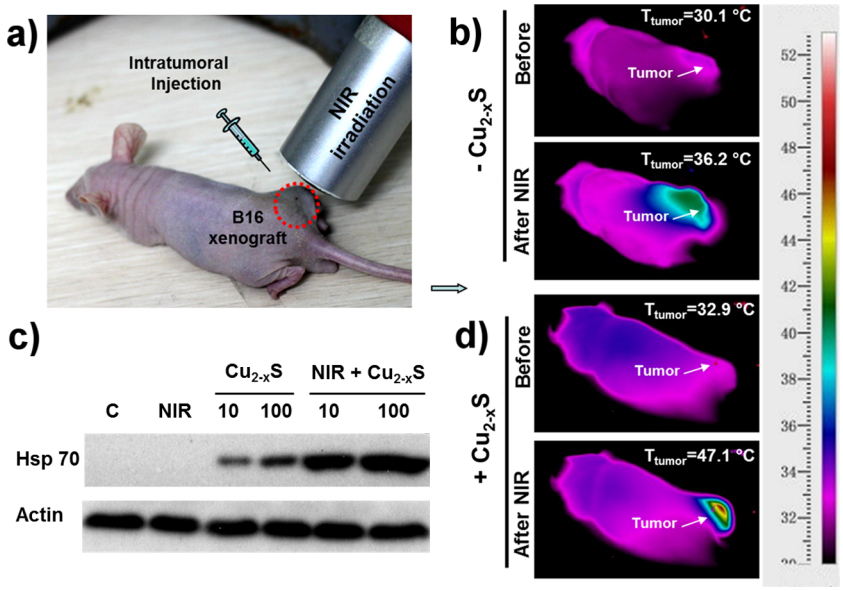

Figure 2. False color infrared thermal images of Balb/c mice bearing a B16 xenograft after 100 s NIR laser irradiation and *in vitro* results for heat shock protein expression. (a) The image of a B16 tumor-bearing Balb/c nude mouse. The NCs were injected intratumorally, followed by NIR irradiation. (b) Infrared thermal images were taken in the nontreated mice before and after NIR irradiation (0.6 W cm^{-2}, 100 s). (c) Western blot analysis of B16 cells after $Cu_{2-x}S$ NCs treatment under NIR (48 h after treatment). Cells were plated at 2×10^5 cells per well in a 6-well plate, treated with $Cu_{2-x}S$ NCs at 10 and 100 μg mL^{-1} (in Cu) with or without NIR (100 s exposure). NIR alone was used as control. The Hsp70 expression was determined by western blotting and normalized using β-actin. (d) Infrared thermal images of the tumor site post injection of $Cu_{2-x}S$ NCs (15 mg kg^{-1}, 0.2 mL) before and after NIR laser light irradiation (0.6 W cm^{-2}, 100 s). The color bar relates to the temperature values in °C.

the laser at a threshold concentration of NCs that led to a final temperature greater than 60 °C. The precipitation could be attributed to the stripping of PEG ligands from the NCs, as confirmed by the increasing values of the Cu/S ratio (from 1.25 to 1.88) measured by ICP-AES and correlated with the loss of thiolated PEG molecules. The aggregation effect, which is activated by light, might be also exploited for maintaining a therapeutic dose of NCs at the irradiation site (*i.e.*, the aggregated size is greater than the tumor fenestration size), thus avoiding NC clearance (a common problem in nanoparticle based solid cancer therapy).[41] On the other hand, it was important to assess if the NC aggregation upon irradiation affected their photothermal efficiency. To simulate this scenario, samples of $Cu_{2-x}S$ NCs at different concentrations were irradiated with NIR laser light at 2.3 W cm^{-2} (spot size 0.4 cm in diameter) for multiple times (up to five cycles). For each heating cycle, NIR light irradiation was applied for 2 min followed by a 2 min cooling period (within which the solutions reached room temperature, see Supporting Information Figure S1b). The result indicated that repeated irradiation did not significantly influence the photothermal properties of the $Cu_{2-x}S$ NCs, even when the temperature was above 60 °C and aggregation occurred.

We monitored the temperature change when the NCs were used as photothermal agents in an *in vivo* mouse model. B16 tumor bearing Balb/c nude mice were intratumorally injected with $Cu_{2-x}S$ NCs (0.2 mL of a NC solution corresponding to 15 mg kg^{-1} in Cu) dissolved in PBS and the photothermal conversion efficacy was measured. Prior to irradiation, the mice were anesthetized with sodium pentobarbital. The temperature increase was monitored by an infrared camera upon irradiation of the tumor region with an 808 nm NIR laser (0.6 W cm^{-2} and a spot size of 2 cm in diameter) for a time lapse of 100 s. For the group of animals that received the $Cu_{2-x}S$ NC injection and were exposed to the laser treatment, the infrared thermal map of the tumor region showed a remarkable temperature increase. After 100 s exposure to the laser the temperature in this group increased by *circa* 14 °C: from 32.9 °C (the initial tumor temperature) up to 47.1 °C (Figure 2d). This was enough to kill the tumor cells in xenografts. One control group of animals was exposed to irradiation but did not receive $Cu_{2-x}S$ NCs and the temperature in the irradiated area was just slightly increased (Figure 2b). Note that the temperature increase was limited to the region containing the NCs and to the spot size of the laser beam. This clearly demonstrates the photothermal efficacy of the $Cu_{2-x}S$ NCs.

To confirm the effect of heat generation induced by the $Cu_{2-x}S$ NCs, we also monitored the heat shock protein 70 (Hsp70) expression *in vitro* in $Cu_{2-x}S$ NCs treated B16 cells with or without NIR irradiation. Hsp70 was selected as a biomarker because it is activated by various stresses, *i.e.*, elevated temperature, environmental stressors and toxicants, including ROS.[42−46] We included NIR light treatment without particles as control. In the presence of NIR irradiation (100 s laser

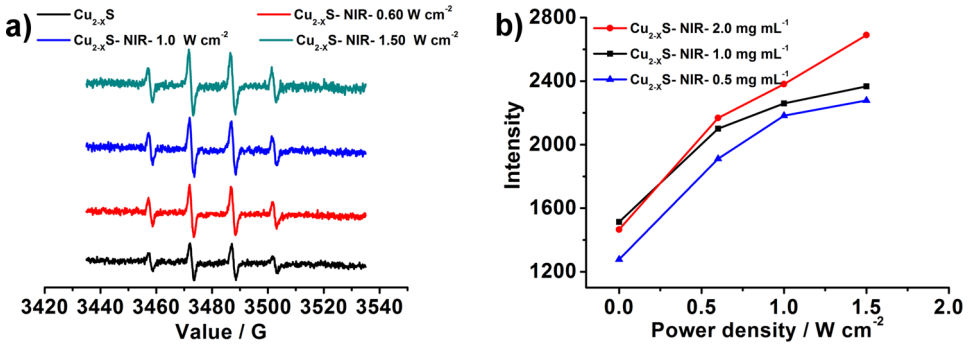

Figure 3. (a) ESR spectrum of $Cu_{2-x}S$ NCs at 2.0 mg mL^{-1} in Cu under different NIR laser power densities (0.6, 1, and 1.5 W cm^{-2}). (b) ESR intensity for the spin trapped hydroxyl radical generated by $Cu_{2-x}S$ NCs at different concentrations (0.5, 1, and 2 mg mL^{-1}) and different laser power densities.

irradiation at wavelength of 808 nm and power density of 0.6 W cm^{-2}), the cells exposed to $Cu_{2-x}S$ NCs expressed significantly more Hsp70 than cells exposed to the particles alone, without NIR irradiation (Figure 2c). A parallel experiment using NIR alone on cells without NCs resulted in very little Hsp70 expression. It is important to mention that we indeed found that $Cu_{2-x}S$ NCs led to marginal increase of Hsp70 *in vitro*. However, what it is more relevant to highlight is that the heat-responsive Hsp70 was significantly increased in the treatment using NIR light plus $Cu_{2-x}S$ NCs in cells (Figure 2c).

Overexpression of Hsp70 can be caused not only by thermal stress, but also by elevated ROS levels.[46] Hence, we investigated by electron spin resonance spectroscopy (ESR) the photodynamic properties of our NCs that could promote the production of the latter. We estimated $^1O_2$ and ·OH generation levels by detecting 2,2,6,6-tetramethylpiperide (TEMP) and 5,5-dimethyl-1-pyrroline-*N*-oxide (DMPO) spin-trapping adducts, which show typical triplet ($^1O_2$) and quadruple (·OH) ESR signals.[47] The $^1O_2$ and ·OH generation of $Cu_{2-x}S$ NCs solutions at concentrations ranging from 0.5 to 2 mg mL^{-1} before and after NIR light irradiation (808 nm, 0.6 W cm^{-2} for 5 min) were investigated. The resulting ESR spectra are reported in Figure 3a, where the 1:2:2:1 multiplicity of the spectra shows the characteristics of a DMPO−OH adduct that is formed by the addition of ·OH to DMPO.[47] Our data suggest that the ROS generation induced by NIR light irradiation of $Cu_{2-x}S$ NCs is both concentration and laser power dependent (Figure 3b). Such a concentration and laser power dependency is a clear sign of photodynamic activity of the $Cu_{2-x}S$ NCs. Aqueous $Cu_{2-x}S$ NCs solutions (2 mg mL^{-1} in Cu) under NIR irradiation (808 nm, 0.6 W cm^{-2}) exhibited up to 83.5% enhanced ·OH levels compared to solutions that were not irradiated by NIR light. However, we observed no obvious ESR signal of $^1O_2$ spin trapped adducts in $Cu_{2-x}S$ NC solutions before and after their irradiation by NIR light (data not shown). It was demonstrated by Kadiiska *et al.* that Cu(I) species in aqueous and biological media produce ROS, mainly through a modified Haber-Weiss cycle.[48] More specifically, it was shown that *in vivo* Cu(II) was reduced *in situ* to Cu(I) by, *e.g.*, ascorbic acid or glutathione, where it reacted with hydrogen peroxide to form Cu(II), hydroxide, and a hydroxyl radical.[48] Under NIR light, Cu(I) ions leaking from the $Cu_{2-x}S$ NCs could undergo similar redox reactions with the surrounding environment.

Additionally, we confirmed the ROS production in NC solutions by a fluorescence assay based on dichlorofluorescein diacetate (DCFH-DA), an oxidation-sensitive fluorescent dye that is often used for intracellular determination of ROS production.[49] The initial, nonfluorescent dye DCFH-DA undergoes a deacetylation reaction to DCFH under basic conditions induced by the Cu(I) release, and can be oxidized by the formed ROS to 2,7-dichlorofluorescein (DCF), which is a highly fluorescent derivative emitting at 529 nm when excited at 495 nm.[50,51]

We exposed solutions of $Cu_{2-x}S$ NCs in water or in buffer at different NC concentrations to laser irradiation (10 min laser irradiation at wavelength of 808 nm with a spot size of 2 cm^2 and power density of 2 W cm^{-2}). Subsequently, the DCFH-DA dye was added and the solution was allowed to equilibrate for 2.5 h. Filtration allowed the separation of the NC fraction from the Cu ions in solution. Besides monitoring the temperature increase of the NC solution, the emission of DCF confirmed that the ROS production was correlated with the concentration of the NCs and with the medium in which the NCs are dispersed.

For the samples at $Cu_{2-x}S$ NC concentration of 0.49 mg mL^{-1} in Cu a ROS formation could be ascertained by the clear absorbance (Figure 4a, red and blue line) and emission signal (Figure 4b, red and blue line) caused by the cleavage of the acetate groups. In this case, the temperature reached 50 °C and no precipitation of the sample, neither in water nor in buffer, was observed. Increasing the $Cu_{2-x}S$ NC concentration up to 1.98 mg mL^{-1} in Cu resulted in heating of the

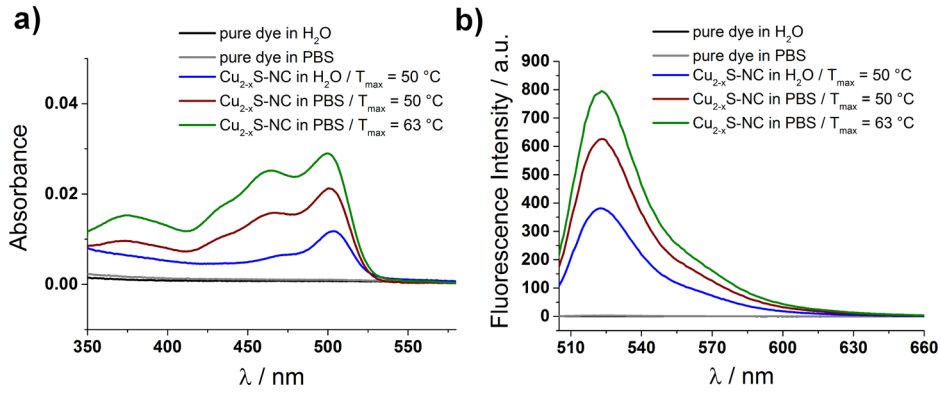

Figure 4. Absorbance (a) and fluorescence (b) spectra (excitation wavelength = 495 nm, slit size 5 nm/5 nm) of reference samples in water and PBS (black and gray line; dye = dichlorofluorescein diacetate), $Cu_{2-x}S$ NCs in water (c(Cu) = 0.49 mg mL^{-1}, blue line), $Cu_{2-x}S$ NCs in PBS (c(Cu) = 0.49 mg mL^{-1}, red line) and $Cu_{2-x}S$ NCs in PBS (irradiation with c(Cu) = 1.98 mg mL^{-1}, absorbance and emission measurements with c(Cu) = 0.49 mg mL^{-1}, green line), after irradiation with a NIR laser at 808 nm (2 W cm^{-2} for 10 min), 2.5 h equilibration time and subsequent filtration.

sample up to 63 °C and a partial agglomeration of the sample, which was also accompanied by a higher emission signal, hence a higher ROS production. At the latter NC concentration, we also measured the release of Cu ions by ICP-AES upon irradiation. After equilibration for 2.5 h and filtration, ICP analysis on the supernatant confirmed a release of copper ions in solution. The measured copper concentration (0.23 mg L^{-1}) corresponds to a release of about 0.012% of the copper present in the initial $Cu_{2-x}S$ NC solution. These data are in agreement with the literature, as it has been reported that the Cu ions in aqueous solutions represent a source of ROS production.[50] It was important to highlight that the ROS production was higher in the case of the sample dissolved in PBS than in pure water. We assume that the presence of salt ions in the buffer facilitates the release of copper from the NCs, as the buffer ions might act as counterions for the copper ions. As expected, no ROS production was found when pure water or buffer solution was exposed to laser irradiation under the same conditions used for the different NC samples.

We have also evaluated the generation of ROS in B16 tumor cells induced by $Cu_{2-x}S$ NCs before and after NIR light irradiation (808 nm, 0.6 W cm^{-2} for 3 min). ROS are generally short-lived macromolecules, such that can oxidize a large variety of macromolecules such as DNA and proteins, which stimulates inflammation and initiates pro-apoptotic cellular signaling, resulting in a high degree of cell damage.[52,53] Herein, dichlorofluorescein diacetate (DCFH-DA) was used to assess intracellular ROS production from $Cu_{2-x}S$ treated B16 cells (particle dose of 25 μg mL^{-1}, 6 h). The DCF fluorescence in B16 cells was evaluated by both fluorescence microscopy and flow cytometry (FCM).[54,55] Figure 5 shows that a much higher DCF fluorescence signal was found in $Cu_{2-x}S$ treated B16 cells (upon irradiation with NIR light) compared to the control group of cells. No obvious DCF fluorescence was

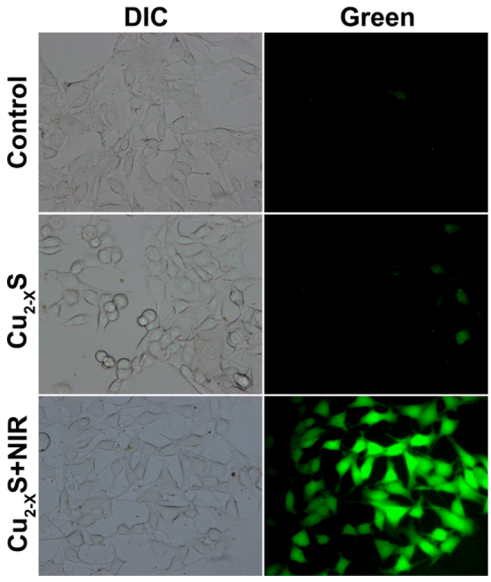

Figure 5. Bright-field and fluorescence images of B16 cells after the co-incubation with $Cu_{2-x}S$ NCs for 6 h. First row: no $Cu_{2-x}S$ NCs, no NIR light. Second row: $Cu_{2-x}S$ NCs at 25 μg mL^{-1}, no NIR light. Third row: $Cu_{2-x}S$ NCs at 25 μg mL^{-1} and NIR light irradiation (808 nm, 0.6W cm^{-2} for 3 min). Green fluorescence indicates high DCF levels, indicating a high ·OH level capable of oxidizing DCFH. Fluorescence intensities are proportional to the ROS concentration.

observed in the control group (no $Cu_{2-x}S$ NCs, no NIR light) and only negligible DCF fluorescence was observed in the $Cu_{2-x}S$ group without NIR. To compare the ROS levels using DCF fluorescence intensity, the confocal visualization was performed using a short exposure time, *i.e.*, 40 ms, which allowed us to clearly discern the differences between $Cu_{2-x}S$ NCs in the presence of NIR irradiation as compared to different controls. The increase in DCF fluorescence intensity is in agreement with ESR data and with the fluorescence assay (Figures 3 and 4), suggesting that the $Cu_{2-x}S$ NCs are engaged in a photodynamic process that induces

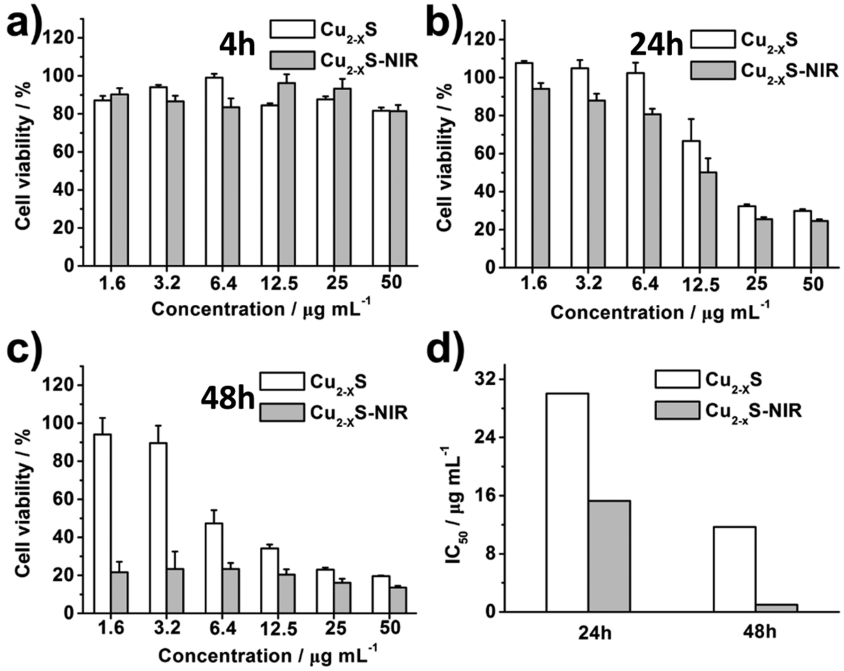

Figure 6. Viability of B16 cells with different concentrations of $Cu_{2-x}S$ NCs with and without NIR irradiation (808 nm, 2.3 W cm^{-2} for 3 min) measured after (a) 4 h, (b) 24 h, and (c) 48 h incubation. (d) Corresponding IC_{50} value of each group for 24 and 48 h.

ROS triggered biological reactions only in the presence of NIR light.

To quantify the ROS generation upon exposure to $Cu_{2-x}S$ NCs, flow cytometry was used to evaluate FCM on B16 cells at different exposure times. Supporting Information Figure S5 shows that, while the intracellular ROS levels increased along with the incubation with NCs, NIR irradiation significantly increased the ROS levels as compared to the treatment using NCs alone. For instance, compared to the $Cu_{2-x}S$ group, ROS levels of the $Cu_{2-x}S$-NIR group increased by 43.2% after treatment with NIR laser light (808 nm, 2.3 W cm^{-2} for 3 min) and incubation for 48 h (Supporting Information Figure S5c). On the basis of these findings, together with ESR measurements, fluorescence assay and fluorescence microscopy, we conclude that the photodynamic properties of our $Cu_{2-x}S$ NCs make them a promising photodynamic agent that allows at the same time for PTT and PDT. Noteworthy, all properties are combined in a few nanometer sized, crystalline entity.

To evaluate and compare the *in vitro* cytotoxicity of $Cu_{2-x}S$ with and without NIR irradiation, the viability of B16 cells was determined by a 2-(4-iodophenyl)-3-(4-nitrophenyl)-5-(2,4-disulfophenyl)-2*H*-tetrazolium (WST-1) assay. As shown in Figure 6, various concentrations of $Cu_{2-x}S$ NCs were incubated with B16 cells for different times (4 h, 24 and 48 h) with and without NIR light irradiation (808 nm, 2.3 W cm^{-2} for 3 min). All experiments evidenced an increasing cytotoxicity against B16 cells in a dose-dependent manner. Both the $Cu_{2-x}S$ and $Cu_{2-x}S$-NIR groups did not show any obvious adverse effect on B16 cells viability for a short incubation time of 4 h. The half-maximum inhibiting concentration (IC_{50} value) of each group is displayed in Figure 6d. The $Cu_{2-x}S$-NIR group exhibited an obvious advantage over the $Cu_{2-x}S$ group in terms of cytotoxicity at all concentrations. The IC_{50} value of the $Cu_{2-x}S$-NIR group was 15.27 μg mL^{-1} in Cu, which is 50.8% lower than the dose for the $Cu_{2-x}S$ group (30.03 μg mL^{-1} in Cu) at 24 h. After 48 h of incubation, this effect was significantly more pronounced. The IC_{50} values of the $Cu_{2-x}S$-NIR group (0.995 μg mL^{-1} in Cu) was about 11 times lower compared to that of the $Cu_{2-x}S$ group (11.69 μg mL^{-1} in Cu), a therapeutic window that allows us to conduct the therapy in a safe fashion. This also clearly proves that the cellular internalization of $Cu_{2-x}S$ is effective at prolonged incubation times, which is a very important parameter for efficient combination of PTT and PDT with potential for cancer therapy. Furthermore, from cytoskeleton organization, we observed that $Cu_{2-x}S$ NCs with NIR irradiation (3 min laser irradiation at wavelength of 808 nm and power density of 0.6 W cm^{-2}) disrupt the cell cytoskeleton, while the control treatments did not cause remarkable cytoskeleton damage (Supporting Information Figure S4).

On the basis of the above analysis, the $Cu_{2-x}S$ NCs show potential as a new class of photosensitizers in addition to previously reported high photothermal conversion,[56−60] which allows for simultaneous treatment by PTT and PDT with one nanoscale crystalline material. We continued to evaluate the *in vivo* efficacy

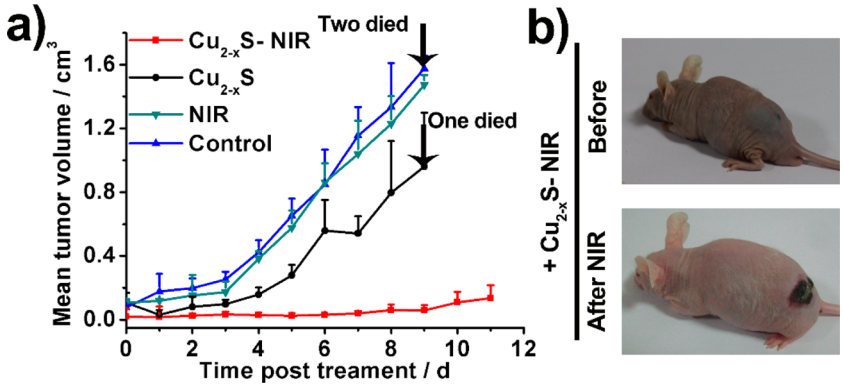

Figure 7. Comparative efficacy study of single intratumoral injection in B16 xenograft bearing nude mouse models. (a) Mean tumor volumes were measured in the control group, NIR group, $Cu_{2-x}S$ group, and $Cu_{2-x}S$-NIR group. (b) Images of B16 bearing nude mice were taken before and at second day with NCs-NIR treatment.

using NCs plus NIR irradiation. To this end, a total of 12 male B16 subcutaneous tumor bearing nude mice were randomly distributed into four groups of three mice per each group: (a) Control group (no NIR, no NCs); (b) NIR group (no NCs, with NIR); (c) $Cu_{2-x}S$ group (NCs, no NIR); and (d) $Cu_{2-x}S$ NIR group (NCs and NIR). The PBS dispersions of $Cu_{2-x}S$ NCs were administered intratumorally (15 mg kg^{-1} in Cu) in groups c and d. The mice in control (a) and the NIR group (b) received the same volume of PBS. Subsequently, the mice in the NIR group (b) and $Cu_{2-x}S$-NIR group (d) were irradiated using NIR laser light (808 nm, 0.6 W cm^{-2}, spot diameter size 2 cm) at tumor site for 3 min immediately post NCs injection. For comparison, the control (a) and the $Cu_{2-x}S$ group (c) mice did not receive NIR exposure. The tumors from the $Cu_{2-x}S$-NIR group (d) appeared as scar at the irradiation site 1 day post NIR exposure (Figure 7b). The use of NCs plus NIR resulted in efficient tumor inhibition, *i.e.*, ~90% inhibition, compared to the controls (Figure 7a). From the survival rate perspective, two mice in control group died after 9 days, due to the invasiveness of B16 carcinoma. This contrasted with the mice in $Cu_{2-x}S$-NIR group (d), which survived during the course of therapy. Interestingly, we also found one animal death in the $Cu_{2-x}S$ group, which is primarily due to the lack of NIR light, resulting in an inefficient therapeutic outcome.

Several studies have highlighted the impact of elevated temperatures on the photodynamic efficiency. An accepted assumption is that a mild hyperthermia treatment can improve the partial oxygen pressure by enhancing the blood flow in tumor tissues.[56] Also, it was found that heat may increase the reactivity of ROS for tumor destruction.[57] Furthermore, some results evidenced that a little damage of proteins in cells, caused by photodynamic therapy, may greatly affect their sensitivity for hyperthermia.[59] Hence, combinatorial PTT and PDT are indeed expected to improve the overall therapeutic effect. It is worth noting that most PSs for PDT are only sensitive to UV−Vis light or to visible light. This is a severe drawback, since biological tissues absorb photons of such high energy, which can results in severe nonspecific side effects. Other NIR active PS like organometallic complexes[18] have lower absorption cross sections than $Cu_{2-x}S$ NCs, making higher laser powers necessary. Our strategy of exploiting PTT with PDT in a single material with a high extinction coefficient at 808 nm ($\varepsilon_{808} = 9.53 \times 10^8$ M^{-1} cm^{-1}) also allows for deeper tissue penetration, which enables the treatment of tumors located deeper in the body.

We also investigated the hemolytic behavior of $Cu_{2-x}S$ NCs at different concentrations with rabbit red blood cells (RBCs, Supporting Information Figure S6). RBCs were isolated from freshly obtained EDTA-stabilized rabbit blood by centrifugation and washing with PBS. Water and PBS were used as the positive and negative controls, respectively. All the solutions were mixed mildly and then kept at room temperature for 3 h. Afterward, the concentration of hemoglobin released from the hemolyzed RBCs was determined by measuring the absorbance of the supernatant at 570 nm using a microplate reader with a reference at 655 nm. The results show that hemolysis of RBCs can be detected only at very high concentrations of 400 μg mL^{-1} (73.2%) and 200 μg mL^{-1} (18.2%) in Cu. At intermediate and low concentrations (below 100 μg mL^{-1} in Cu), no obvious hemolytic RBCs (<4.1%) can be detected.

With the purpose of an accurate assessment of the $Cu_{2-x}S$ NC toxicity *in vivo*, a series of doses was set for the *in vivo* toxicity studies of $Cu_{2-x}S$ NCs following the method provided by the Organization for Economic Cooperation and Development (OECD, guideline 425, Supporting Information Figure S7a). The first mouse received a dose one step below the assumed estimate of the MTD. If the animal survived, the second animal received a higher dose. If the first animal died, the second animal received a lower dose. The signs of toxicity or anaphylactic response after injection of NCs were recorded following US Pharmacope.[58] The doses

with 200, 150, 100, 50, and 25 mg kg^{-1} in Cu were administered *via* iv injection in a single dose, followed by a 48 h observation period. The first mouse received 200 mg kg^{-1} in Cu and died 15 min post iv injection. The second mouse received 150 mg kg^{-1} and died after 40 h post injection. The third mouse of 100 mg kg^{-1} also died in 46 h. The forth mouse received 50 and 25 mg kg^{-1} and did not show any toxic reaction during the following observation. Body weights and clinic manifestation were observed and recorded carefully throughout the experimental period. After 7 days, tissues recovered from the necropsy were fixed in 10% formalin, embedded in paraffin, sectioned, and stained with hematoxylin and eosin (H&E) for histological examination using standard techniques. As depicted in Supporting Information Figure S7b, no abnormalities were found in the liver, spleen, kidney, lung and brain of $Cu_{2-x}S$ treated-mice intravenously at 25 and 50 mg kg^{-1}. However, treatment with $Cu_{2-x}S$ NCs at 100 and 150 mg kg^{-1} led to degenerative necrosis and disappearance of hepatocytes. Also, evidence of liver organization hyperemia was observed and marginal zones of the spleen were destroyed by $Cu_{2-x}S$ NCs at 150 mg kg^{-1} in Cu. In addition, we observed necrosis and disappearance of the lymphocyte in the marginal zone, along with the increase of the hemosiderin. Treatment with 200 mg kg^{-1} in Cu of $Cu_{2-x}S$ NCs lead to hepatocytes in different degrees of cell shrinkage and chromatin condensation. The histological examination indicated that the liver and spleen were the primary involved targeting organs of $Cu_{2-x}S$ treatment at high dose. The lower dose of 50 mg kg^{-1} was considered as the maximum tolerated dose (MTD) for $Cu_{2-x}S$ NCs.

CONCLUSION

In this *in vitro* and *in vivo* study, we report for the first time on the dual PTT and PDT cytotoxic effects of NIR plasmonic copper sulfide ($Cu_{2-x}S$) NCs when illuminated by NIR laser light. We can ascribe the therapeutic effect to a combination of PTT and PDT, rather than PPT alone. ROS generation upon NIR excitation of $Cu_{2-x}S$ NCs was proven both by ESR spectroscopy and DCF fluorescence assays. We have shown that the PEG-coated $Cu_{2-x}S$ NCs have a reasonable biocompatibility, good photothermal conversion efficiency, and unique photodynamic capability under NIR laser light illumination. We also evaluated the maximum tolerated dose of $Cu_{2-x}S$ NCs. We believe that this work will catalyze further investigations on the different therapeutic mechanisms elicited by plasmonic copper chalcogenide NCs. The advantage of copper sulfide NCs lays in their small size, which leads to the possibility of deeper tissue permeation and additionally in their high extinction coefficients in the NIR region. Further studies in this direction may consider for example the photodynamic effects of copper chalcogenide NCs in hypoxic tumors therapy.

EXPERIMENTAL SECTION

Chemicals for Synthesis and Water Transfer of Nanocrystals. Cu(I)Cl (99.999%), and sulfur powder (99%) were purchased from Strem Chemicals. Oleylamine (70%) and 1-octadecene (90%) were purchased from Sigma-Aldrich. Toluene (anhydrous) and ethanol (anhydrous) were purchased from Carlo Erba. α-Methoxy-ω-mercapto PEG (CH_3O-PEG-SH PEG, MW 2000 Da) was purchased from Rapp Polymere (product code 122000-40). α-Mercapto-ω-carboxy PEG (HS-C_2H_4-CONH-PEG-O-C_3H_6-COOH PEG, MW 3000 Da) was purchased from Rapp Polymere (product code: 133000-4-32).

Synthesis of $Cu_{2-x}S$ Nanocrystals. Copper sulfide NCs were synthesized according to our recent approaches for alloyed NCs with modifications.[29] In detail, first, the copper ion solution was prepared by dissolving 4 mmol copper(I) chloride in 24 mL oleylamine at 100 °C, using standard Schlenk line techniques. When all the copper(I) chloride was dissolved, the above solution was allowed to cool to room temperature. The sulfur stock solution was prepared by dissolving 2 mmol sulfur powder in 8 mL octadecene (ODE) at 180 °C, under nitrogen, until all the power was dissolved and the color of the solution became transparent yellow. The copper and sulfur stock solutions were mixed at room temperature and were then heated to 180 °C at the rate of 10 °C/min under nitrogen. After the temperature was kept at 180 °C for 15 min, the reaction mixture was cooled to room temperature. 10 mL of toluene was added followed by the addition of an excess of ethanol to precipitate the $Cu_{2-x}S$ NCs, which were washed once more and finally dispersed in 40 mL of chloroform for further processing. The yield of NCs was estimated by ICP-AES to be around 70%, which can guarantee the production of 200 mg in one synthesis batch.

Ligand Exchange Procedure. A 5 mL $Cu_{2-x}S$ NCs solution ([Cu] = 2 mg mL^{-1} in $CHCl_3$ as measured by ICP-AES) was diluted with 15 mL toluene and mixed with a solution of 80 mg HS-PEG-OMe (M_w = 2 kDa) and 20 mg HS-PEG-COOH (M_w = 3 kDa) in 1 mL of toluene. The mixture was filled in a separating funnel and mixed by gentle shaking. After addition of 10 mL Milli-Q water, the two phases were emulsified by gentle shaking. The mixture was let to stand until complete phase separation and the aqueous phase was collected which contained the ligand exchanged $Cu_{2-x}S$@HS-PEG NCs. This procedure was repeated two times to completely transfer all NCs to the aqueous phase. The combined aqueous phases were filled in a round-bottom flask and any remaining toluene was removed under reduced pressure at 40 °C at 77 mbar for 1 h. For the purification from unbound HS-PEG, the solution was filled in a cellulose acetate membrane tubing (molecular cutoff = 50 kDa) and dialyzed against 5 L Milli-Q water overnight. Washing with water was performed 5 times. Finally, the NCs solution was withdrawn from the membrane tubing and concentrated in Amicon centrifuge tubes (15 mL, molecular cutoff = 100 kDa) at 3500 rpm. The Cu/S contents were determined by ICP-AES and the sample was stored at 4 °C before usage.

Irradiation with NIR-Laser and ROS Detection in NCs Dispersion. For the irradiation of the samples, a CW laser diode emitting in the NIR at 808 nm (Roithner RLTMDL-808-5W-5), focused on a spot size of 2 cm^2 with a power of 4 W (power density 2 W cm^{-2}), was used.

Please notice that although the $Cu_{2-x}S$ NCs have a much higher absorption at 1400 nm, at this wavelength water absorbs strongly too, which will lead to nonspecific tissue heating. Therefore, the laser study was carried out at 808 nm where the $Cu_{2-x}S$ NCs could still heat and the water absorption was

minimized. For the ROS detection, different $Cu_{2-x}S$-NC samples were prepared either in water or in PBS (NC concentration fixed at 0.49 mg mL^{-1} of Cu) and a 1 mL solution of each sample was irradiated for 10 min at a power density of 2 W cm^{-2}. To detect the ROS production, upon incubation with fluorescein diacetate in ethanol (6 mg mL^{-1}; 250 mmol) for 2.5 h, the reaction mixture was filtered by centrifugation (5 min, 3000 rpm, filter cutoff 100 kDa) and the clear solution was analyzed by UV−vis and fluorescence spectroscopy.

The most concentrated NC sample (1.98 mg mL^{-1} in Cu) in 0.5 mL PBS was irradiated for 10 min at a power density of 2 W cm^{-2}. Subsequently, 250 μL of the mixture was diluted in 750 μL PBS resulting in a concentration of Cu equal to 0.49 mg mL^{-1} to ensure comparable results. Afterward, 100 μL of a dichlorofluorescein diacetate (DCFH-DA) solution in ethanol (6 mg mL^{-1}; 250 mmol) was added to each sample and the mixture was allowed to equilibrate for 2.5 h. Subsequently, the solution was filtered by centrifugation (5 min, 3000 rpm, filter cutoff of 100 000 g mol^{-1}) and the clear solution was analyzed by UV−vis and fluorescence spectroscopy. The UV−vis spectra were recorded on a Cary 5000 spectrophotometer whereas emission spectra were recorded on a Cary Eclipse fluorescence spectrophotometer.

Characterization of the Nanocrystals. The morphology and the structure of the resulting NCs were observed with JEM-2100 electron microscope (TEM) and JEM-2100F high-resolution transmission electron microscopy (HRTEM), operating at 200 kV. UV−vis-NIR extinction spectra of $Cu_{2-x}S$ were recorded on either a JASCO UV/vis 570 or a Cary 5000 UV−vis-NIR photospectrometer. The Cu/S ratios were determined by inductively couple plasma atomic emission spectrometry (ICP-AES, Thermo Fisher iCAP 6000). The crystal structure of the $Cu_{2-x}S$ NCs was inferred from X-ray diffraction (XRD, Rigaku Smart Lab) by using graphite monochromatised Cu Kα radiation (λ = 1.5418 Å). DLS experiments were carried out with a Malvern Zetasizer (Nano ZS series, Malvern Instruments Ldt, England).

Measurement of Photothermal Effects. The photothermal conversion efficiency of the $Cu_{2-x}S$ NCs in PBS at different concentrations (1.6, 3.2, 6.4, 12.5, 25, 50, 100, and 200 μg mL^{-1}) was determined using laser light at 808 nm with a power density of 2.3 W cm^{-2}. A CW GCSLS-05−007 semiconductor laser device (Daheng New Epoch Technology, Inc., Beijing, China) was used, with a center wavelength of 808 ± 10 nm. An optical fiber was used to transfer laser light from the laser unit to a cuvette containing the $Cu_{2-x}S$ NCs (1 mL). The temperature of the solution was detected with a PT-3S thermo-detector (Optex Co., Ltd., Japan). The detailed protocol is descried in the Supporting Information. Repeated heat/cool cycles were performed with the same instrument. The $Cu_{2-x}S$ NCs were irradiated multiple times with NIR light for 2 min, followed by a 2 min cooling period. The temperature data points were recorded at 1 min intervals.

ESR Measurements. Electron spin resonance (ESR, recorded on a ESP300E spectrometer) was used to estimate $^1O_2$ and ·OH generation by detecting 2,2,6,6-tetramethylpiperide (TEMP) and 5,5-dimethyl-1-pyrroline-*N*-oxide (DMPO) spin-trapping adduct, which have typical triplet ($^1O_2$) and/or quadruple ESR signals (·OH). Spectra of spin trapped ·OH were obtained by mixing 20 μL DMPO with 100 μL $Cu_{2-x}S$ NCs solution at various concentrations. Then samples were injected into quartz capillaries designed especially for ESR analysis and directly irradiated inside the cavity of the ESR spectrometer with different laser power densities (0.6, 1.0, and 1.5 W cm^{-2} at 808 nm) for 5 min. The ESR spectra of the $Cu_{2-x}S$ NCs in the presence of DMPO without irradiation were collected as controls.

Western Blotting. B16 cells were plated at 2 × 10^5 cells per well in a 6-well plate. The cells were treated with $Cu_{2-x}S$ NCs at 10 and 100 μg mL^{-1} with or without NIR (100 s exposure at wavelength of 808 nm and power density of 0.6 W cm^{-2}) and were incubated for additional 48 h. NIR alone was used as control. The Hsp70 expression was determined by Western blotting and normalized using β-actin. Briefly, the cells were washed in PBS and the pellets lysed in a buffer containing Triton X-100 and protease inhibitors. Forty micrograms of total protein was electrophoresed by SDS-PAGE and transferred to a PVDF membrane. The membranes were incubated with primary antibody to Hsp70, followed by secondary antibody incubation, before the addition of the HRP-conjugated streptavidin−biotin complex. The proteins were detected using ECL reagent according to the manufacturer's instructions.

Determination of Intracellular Reactive Oxygen Species (ROS). *Fluorescence Images.* B16 cells were seeded on glass-bottom dishes (35 mm, kindly provided by MatTek Corporation) for 24 h to allow the cells to attach to the surface of the wells. After treatment with $Cu_{2-x}S$ NCs (25 μg mL^{-1}, 1 mL) for 6 h, the cells were washed three times in phosphate-buffered saline (PBS). Then they were cultured with dichlorofluorescein diacetate (DCFH-DA) (10 μmol L^{-1}) at 37 °C for 50 min. Cells were washed again three times with PBS before the $Cu_{2-x}S$-NIR group was irradiated by NIR laser light (808 nm, 0.6 W cm^{-2}) for 3 min. Intracellular ROS was detected by means of DCFH which could be oxidized to a highly fluorescent derivative, 2,7-dichloro-fluorescein (DCF) in the presence of hydroxyl (·OH) radicals. Then DCF fluorescence was detected by a Nikon fluorescence microscope (Nikon Eclipse Ti−S, CCD: Ri1). Attempts to detect $^1O_2$ were made by using the same method.

Flow Cytometry. B16 cells (5 × 10^5 cells) were incubated with the RPMI-1640 medium dispersion of $Cu_{2-x}S$ NCs (25 μg mL^{-1}) for 0, 24, and 48 h. Then, the excess of noninternalized $Cu_{2-x}S$ NCs was removed by washing several times with PBS. Cells were cultured with DCFH-DA (10 μmol L^{-1}) at 37 °C for 50 min and washed with PBS. One group was trypsinized and collected in 1 mL PBS after NIR irradiation (808 nm, 0.6 W cm^{-2}) for 3 min. The other group as a control was not irradiated with NIR laser light. Fluorescent stained cells were transferred to polystyrene tubes for acquisition and analysis by Flow cytometry (BD FACS Calibur).

In Vitro Cytotoxicity. B16 cells were seeded in 96-well plates (10^4 cells/well, 100 μL) and incubated for 24 h to allow the cells to attach to the surface of the wells, then they were exposed to different concentrations of $Cu_{2-x}S$ NCs (1.6, 3.2, 6.4, 12.5, 25, and 50 μg mL^{-1}). One of the $Cu_{2-x}S$ groups was examined after irradiation with an 808 nm CW laser (2.3 W cm^{-2}, 3 min). The other group was not irradiated. To exclude other possible influences of $Cu_{2-x}S$ NCs and $Cu_{2-x}S$ + NIR on B16 cell viability, respectively, various concentrations of $Cu_{2-x}S$ NCs were incubated with B16 cells at 37 °C for different times (4, 24, and 48 h). Cell viability was measured using the WST assay according to the procedures suggested by the manufacturer. Next, absorbance at 450 nm was measured against a background, which served as blank, using a microtiter plate reader (Thermo Fisher CO.). The data reported represent the means of quadruplicate measurements and error bars display the standard deviation.

Staining for Cell Cytoskeleton and Nucleus. B16 cells were dispensed into a Coverglass-Bottom Dish (1.5 × 10^4 cells/well, 200 μL). After allowing them to attach for 24 h, $Cu_{2-x}S$ NCs solutions (50 μg mL^{-1} in Cu) were diluted appropriately in fresh media and added to the microwells (1 mL). Cells were incubated for 4 h at 37 °C in the presence of 5% CO_2. The medium was removed and the cells were washed two times with the RPMI-1640 medium not containing FBS. Then, cells were irradiated for 3 min with NIR light (808 nm, 0.6 W cm^{-2}). The nucleus was counterstained with 4′,6-diamidino-2-phenylindole and cell microfilament were stained by Actin-Tracker Green. Micrographs of cells were then taken using Confocal laser scanning microscopy (CLSM).

Animal Preparation. All animal experiments were performed in compliance with the local ethics committee. ICR mice and Balb/c nude mice (provided by Vital River Laboratory Animal Technology Co. Ltd.), aged 6−8 weeks, were used in the experiments. Groups of five same sex mice were housed in stainless steel cages containing sterile paddy husk as bedding in ventilated animal rooms. They were acclimated in the controlled environment (temperature: 22 ± 1 °C; humidity: 60 ± 10% and light: 12 h light/dark cycle) with free access to water and a commercial laboratory complete food. The mice were injected subcutaneously in the hind part with 0.2 mL of a suspension containing 4 × 10^6 B16 cells.

Infrared Thermal Imaging. A Balb/c nude mouse was injected with $Cu_{2-x}S$ NC PBS solution (15 mg kg^{-1} in Cu) intratumorally

to measure the photothermal effect by an infrared thermal mapping apparatus by irradiating the tumor region with NIR laser light at 808 nm (0.6 W cm^{-2}) for 100 s. As a control, a nude mouse which received no NCs was also irradiated and monitored under the same conditions. All nude mice were anesthetized with iv injection of sodium pentobarbital (0.2 mL) prior to the irradiation treatment.

***In Vivo* Antitumor Activity.** A total of 12 male mice bearing B16 tumors were randomly distributed into four groups: (a) Control group, (b) NIR group, (c) $Cu_{2-x}S$ group, and (d) $Cu_{2-x}S$-NIR group. Each group consisted of three mice. The PBS dispersion of $Cu_{2-x}S$ NCs was administered intratumorally (15 mg kg^{-1} in Cu) in the groups c and d. The control and NIR group had an equivalent volume of PBS. Then the $Cu_{2-x}S$-NIR and the NIR groups were irradiated in the tumor region with NIR laser light (808 nm, 0.6 W cm^{-2}) for 3 min directly after injection. The control group and $Cu_{2-x}S$ group were not irradiated. Tumor volumes were determined according to the formula $(a \times b^2)/2$, where a and b are the long and short diameters of a tumor, respectively.

Hemolysis Assay. RBCs were isolated from freshly obtained ethylenediamine tetraacetic acid (EDTA)-stabilized rabbit blood by centrifugation and washing with PBS. Water and PBS were used as the positive and negative controls, respectively. Aliquots of 0.2 mL of diluted RBC suspension were added to 0.8 mL of PBS solutions containing different concentrations of $Cu_{2-x}S$ NCs. All the sample tubes were mixed mildly and then kept standing at room temperature for 3 h. Then, the concentration of hemoglobin released from the hemolyzed RBCs was determined by measuring the absorbance of the supernatant at 570 nm using a microplate reader while using the absorbance at 655 nm as reference. The percent of RBC hemolysis was calculated by using the following formula: % hemolysis = (sample absorbance − negative control absorbance)/(positive control absorbance − negative control absorbance) × 100.

***In Vivo* Systematic Toxicity.** A total of 5 healthy mice were used in this experiment. The first mouse received a dose one step below the assumed estimate of the MTD. If the animal survived, the second animal received a higher dose. If the first animal died, the second animal received a lower dose. The signs of toxicity or anaphylactic response after injection of NCs were recorded following US Pharmacope.[56] The doses of 200, 150, 100, 50, and 25 mg kg^{-1} were iv administered in a single dose to only one animal, followed by a 48 h observation period. Body weights and clinical manifestations were observed and recorded carefully throughout the experiment period. After 7 days, tissues recovered from the necropsy were fixed in 10% formalin, embedded in paraffin, sectioned, and stained with hematoxylin and eosin (H&E) for histological examination using standard techniques. After hematoxylin eosin staining, the slides were observed and images were taken using an optical microscope (Nikon Eclipse Ti−S, CCD: Ri1).

Conflict of Interest: The authors declare no competing financial interest.

Supporting Information Available: Heat/cool experiments of $Cu_{2-x}S$ NCs aqueous solutions under various conditions and related DLS characterization; estimation of the photothermal efficiency; confocal cell studies under NIR irradiation and related ROS estimations; hemolysis tests for $Cu_{2-x}S$ NCs; *ex vivo* histological chacterizations of various organ tissues. This material is available free of charge *via* the Internet at http://pubs.acs.org.

Acknowledgment. This work was supported by Beijing Nova Program (Z111103054511113), the National Natural Science Foundation of China (No. 31271075, 81201814, 31270022, 81471784, 51202260, 31400854) and the National Hi-Technology Research and Development Program (863 Program) (No. 2013AA032201, 2012AA022701 and 2011AA02A114).

REFERENCES AND NOTES

1. Fang, J.; Seki, T.; Maeda, H. Therapeutic Strategies by Modulating Oxygen Stress in Cancer and Inflammation. *Adv. Drug Delivery Rev.* **2009**, *61*, 290–302.
2. Kehrer, J. P. Free Radicals as Mediators of Tissue Injury and Disease. *Chem. Rev. Toxicol.* **1993**, *23*, 21–48.
3. Nioka, S.; Chance, B. Nir Spectroscopic Detection of Breast Cancer. *Technol. Cancer Res. Treat.* **2005**, *4*, 497–512.
4. Bonnett, R. Photosensitizers of the Porphyrin and Phthalocyanine Series for Photodynamic Therapy. *Chem. Soc. Rev.* **1995**, *24*, 19–33.
5. Yang, H. Y.; Wang, F. Y.; Zhang, Z. Y. Photobleaching of Chlorins in Homogeneous and Heterogeneous Media. *Dyes Pigm.* **1999**, *43*, 109–117.
6. Bechet, D.; Couleaud, P.; Frochot, C.; Viriot, M. L.; Guillemin, F.; Barberi-Heyob, M. Nanoparticles as Vehicles for Delivery of Photodynamic Therapy Agents. *Trends Biotechnol.* **2008**, *26*, 612–621.
7. Velusamy, M.; Shen, J. Y.; Lin, J. T.; Lin, Y. C.; Hsieh, C. C.; Lai, C. H.; Lai, C. W.; Ho, M. L.; Chen, Y. C.; Chou, P. T.; et al. A New Series of Quadrupolar Type Two-Photon Absorption Chromophores Bearing 11, 12-Dibutoxydibenzo[a,C]-Phenazine Bridged Amines; Their Applications in Two-Photon Fluorescence Imaging and Two-Photon Photodynamic Therapy. *Adv. Funct. Mater.* **2009**, *19*, 2388–2397.
8. Sitnik, T. M.; Hampton, J. A.; Henderson, B. W. Reduction of Tumour Oxygenation During and after Photodynamic Therapy *in Vivo*: Effects of Fluence Rate. *Br. J. Cancer* **1998**, *77*, 1386–1394.
9. Borroni, R. G.; Carugno, A.; Rivetti, N.; Arbustini, E.; Brazzelli, V. Risk of Acute Postoperative Hypertension after Topical Photodynamic Therapy for Non-Melanoma Skin Cancer. *Photodermatol. Photoimmunol. Photomed.* **2013**, *29*, 73–77.
10. Riedinger, A.; Guardia, P.; Curcio, A.; Garcia, M. A.; Cingolani, R.; Manna, L.; Pellegrino, T. Subnanometer Local Temperature Probing and Remotely Controlled Drug Release Based on Azo-Functionalized Iron Oxide Nanoparticles. *Nano Lett.* **2013**, *13*, 2399–2406.
11. El-Sayed, I. H.; Huang, X. H.; El-Sayed, M. A. Surface Plasmon Resonance Scattering and Absorption of Anti-Egfr Antibody Conjugated Gold Nanoparticles in Cancer Diagnostics: Applications in Oral Cancer. *Nano Lett.* **2005**, *5*, 829–834.
12. Huang, X. H.; El-Sayed, I. H.; Qian, W.; El-Sayed, M. A. Cancer Cell Imaging and Photothermal Therapy in the Near-Infrared Region by Using Gold Nanorods. *J. Am. Chem. Soc.* **2006**, *128*, 2115–2120.
13. Chen, J. Y.; Yang, M. X.; Zhang, Q. A.; Cho, E. C.; Cobley, C. M.; Kim, C.; Glaus, C.; Wang, L. H. V.; Welch, M. J.; Xia, Y. N. Gold Nanocages: A Novel Class of Multifunctional Nanomaterials for Theranostic Applications. *Adv. Funct. Mater.* **2010**, *20*, 3684–3694.
14. Liu, H. Y.; Chen, D.; Li, L. L.; Liu, T. L.; Tan, L. F.; Wu, X. L.; Tang, F. Q. Multifunctional Gold Nanoshells on Silica Nanorattles: A Platform for the Combination of Photothermal Therapy and Chemotherapy with Low Systemic Toxicity. *Angew. Chem., Int. Ed.* **2011**, *50*, 891–895.
15. Liu, H. Y.; Liu, T. L.; Li, L. L.; Hao, N. J.; Tan, L. F.; Meng, X. W.; Ren, J.; Chen, D.; Tang, F. Q. Size Dependent Cellular Uptake, *in Vivo* Fate and Light-Heat Conversion Efficiency of Gold Nanoshells on Silica Nanorattles. *Nanoscale* **2012**, *4*, 3523–3529.
16. Liu, H. Y.; Liu, T. L.; Wu, X. L.; Li, L. L.; Tan, L. F.; Chen, D.; Tang, F. Q. Targeting Gold Nanoshells on Silica Nanorattles: A Drug Cocktail to Fight Breast Tumors *via* a Single Irradiation with near-Infrared Laser Light. *Adv. Mater.* **2012**, *24*, 755–761.
17. Tian, B.; Wang, C.; Zhang, S.; Feng, L. Z.; Liu, Z. Photothermally Enhanced Photodynamic Therapy Delivered by Nano-Graphene Oxide. *ACS Nano* **2011**, *5*, 7000–7009.
18. Jang, B.; Park, J. Y.; Tung, C. H.; Kim, I. H.; Choi, Y. Gold Nanorod-Photosensitizer Complex for Near-Infrared Fluorescence Imaging and Photodynamic/Photothermal Therapy *in Vivo*. *ACS Nano* **2011**, *5*, 1086–1094.
19. Gao, L.; Fei, J.; Zhao, J.; Li, H.; Cui, Y.; Li, J. Hypocrellin-Loaded Gold Nanocages with High Two-Photon Efficiency for Photothermal/Photodynamic Cancer Therapy *in Vitro*. *ACS Nano* **2012**, *6*, 8030–8040.

20. Lin, J.; Wang, S.; Huang, P.; Wang, Z.; Chen, S.; Niu, G.; Li, W.; He, J.; Cui, D.; Lu, G.; et al. Photosensitizer-Loaded Gold Vesicles with Strong Plasmonic Coupling Effect for Imaging-Guided Photothermal/Photodynamic Therapy. *ACS Nano* **2013**, *7*, 5320–5329.
21. Comin, A.; Manna, L. New Materials for Tunable Plasmonic Colloidal Nanocrystals. *Chem. Soc. Rev.* **2014**, *43*, 3957–3975.
22. Faucheaux, J. A.; Stanton, A. L. D.; Jain, P. K. Plasmon Resonances of Semiconductor Nanocrystals: Physical Principles and New Opportunities. *J. Phys. Chem. Lett.* **2014**, *5*, 976–985.
23. Jain, P. K.; Manthiram, K.; Engel, J. H.; White, S. L.; Faucheaux, J. A.; Alivisatos, A. P. Doped Nanocrystals as Plasmonic Probes of Redox Chemistry. *Angew. Chem., Int. Ed.* **2013**, *52*, 13671–13675.
24. Luther, J. M.; Jain, P. K.; Ewers, T.; Alivisatos, A. P. Localized Surface Plasmon Resonances Arising from Free Carriers in Doped Quantum Dots. *Nat. Mater.* **2011**, *10*, 361–366.
25. Hsu, S.-W.; On, K.; Tao, A. R. Localized Surface Plasmon Resonances of Anisotropic Semiconductor Nanocrystals. *J. Am. Chem. Soc.* **2011**, *133*, 19072–19075.
26. Xie, Y.; Riedinger, A.; Prato, M.; Casu, A.; Genovese, A.; Guardia, P.; Sottini, S.; Sangregorio, C.; Miszta, K.; Ghosh, S.; et al. Copper Sulfide Nanocrystals with Tunable Composition by Reduction of Covellite Nanocrystals with Cu^{+} Ions. *J. Am. Chem. Soc.* **2013**, *135*, 17630–17637.
27. Xie, Y.; Carbone, L.; Nobile, C.; Grillo, V.; D'Agostino, S.; Della Sala, F.; Giannini, C.; Altamura, D.; Oelsner, C.; Kryschi, C. et al. Metallic-Like Stoichiometric Copper Sulfide Nanocrystals: Phase- and Shape-Selective Synthesis, near-Infrared Surface Plasmon Resonance Properties, and Their Modeling. *ACS Nano* **2013**, *7*, 7352–7369.
28. Mendelsberg, R. J.; Garcia, G.; Li, H. B.; Manna, L.; Milliron, D. J. Understanding the Plasmon Resonance in Ensembles of Degenerately Doped Semiconductor Nanocrystals. *J. Phys. Chem. C* **2012**, *116*, 12226–12231.
29. Zhao, Y. X.; Pan, H. C.; Lou, Y. B.; Qiu, X. F.; Zhu, J. J.; Burda, C. Plasmonic $Cu_{2-x}S$ Nanocrystals: Optical and Structural Properties of Copper-Deficient Copper(I) Sulfides. *J. Am. Chem. Soc.* **2009**, *131*, 4253–4261.
30. Saldanha, P. L.; Brescia, R.; Prato, M.; Li, H.; Povia, M.; Manna, L.; Lesnyak, V. Generalized One-Pot Synthesis of Copper Sulfide, Selenide-Sulfide, and Telluride-Sulfide Nanoparticles. *Chem. Mater.* **2014**, *26*, 1442–1449.
31. Dorfs, D.; Hartling, T.; Miszta, K.; Bigall, N. C.; Kim, M. R.; Genovese, A.; Falqui, A.; Povia, M.; Manna, L. Reversible Tunability of the near-Infrared Valence Band Plasmon Resonance in $Cu_{2-x}Se$ Nanocrystals. *J. Am. Chem. Soc.* **2011**, *133*, 11175–11180.
32. Kriegel, I.; Jiang, C. Y.; Rodriguez-Fernandez, J.; Schaller, R. D.; Talapin, D. V.; da Como, E.; Feldmann, J. Tuning the Excitonic and Plasmonic Properties of Copper Chalcogenide Nanocrystals. *J. Am. Chem. Soc.* **2012**, *134*, 1583–1590.
33. Tian, Q. W.; Jiang, F. R.; Zou, R. J.; Liu, Q.; Chen, Z. G.; Zhu, M. F.; Yang, S. P.; Wang, J. L.; Wang, J. H.; Hu, J. Q. Hydrophilic Cu_9S_5 Nanocrystals: A Photothermal Agent with a 25.7% Heat Conversion Efficiency for Photothermal Ablation of Cancer Cells *in Vivo*. *ACS Nano* **2011**, *5*, 9761–9771.
34. Hessel, C. M.; Pattani, V. P.; Rasch, M.; Panthani, M. G.; Koo, B.; Tunnell, J. W.; Korgel, B. A. Copper Selenide Nanocrystals for Photothermal Therapy. *Nano Lett.* **2011**, *11*, 2560–2566.
35. Zhou, M.; Zhang, R.; Huang, M. A.; Lu, W.; Song, S. L.; Melancon, M. P.; Tian, M.; Liang, D.; Li, C. A Chelator-Free Multifunctional [^{64}Cu]-CuS Nanoparticle Platform for Simultaneous Micro-Pet/Ct Imaging and Photothermal Ablation Therapy. *J. Am. Chem. Soc.* **2010**, *132*, 15351–15358.
36. Ding, X.; Liow, C. H.; Zhang, M.; Huang, R.; Li, C.; Shen, H.; Liu, M.; Zou, Y.; Gao, N.; Zhang, Z.; et al. Surface Plasmon Resonance Enhanced Light Absorption and Photothermal Therapy in the Second near-Infrared Window. *J. Am. Chem. Soc.* **2014**, *136*, 15684–15693.
37. Weissleder, R. A Clearer Vision for *in Vivo* Imaging. *Nat. Biotechnol.* **2001**, *19*, 316–317.
38. Wu, Y.; Wadia, C.; Ma, W. L.; Sadtler, B.; Alivisatos, A. P. Synthesis and Photovoltaic Application of Copper(I) Sulfide Nanocrystals. *Nano Lett.* **2008**, *8*, 2551–2555.
39. Roper, D. K.; Ahn, W.; Hoepfner, M. Microscale Heat Transfer Transduced by Surface Plasmon Resonant Gold Nanoparticles. *J. Phys. Chem. C* **2007**, *111*, 3636–3641.
40. Bhattacharyya, S.; Kudgus, R.; Bhattacharya, R.; Mukherjee, P. Inorganic Nanoparticles in Cancer Therapy. *Pharm. Res.* **2011**, *28*, 237–259.
41. Cho, Y. W.; Park, S. A.; Han, T. H.; Son, D. H.; Park, J. S.; Oh, S. J.; Moon, D. H.; Cho, K.-J.; Ahn, C.-H.; Byun, Y.; et al. *In Vivo* Tumor Targeting and Radionuclide Imaging with Self-Assembled Nanoparticles: Mechanisms, Key Factors, and Their Implications. *Biomaterials* **2007**, *28*, 1236–1247.
42. Schildkopf, P.; Frey, B.; Ott, O. J.; Rubner, Y.; Multhoff, G.; Sauer, R.; Fietkau, R.; Gaipl, U. S. Radiation Combined with Hyperthermia Induces Hsp70-Dependent Maturation of Dendritic Cells and Release of Pro-Inflammatory Cytokines by Dendritic Cells and Macrophages. *Radiother. Oncol.* **2011**, *101*, 109–115.
43. Morimoto, R. I. Cells in Stress: Transcriptional Activation of Heat Shock Genes. *Science* **1993**, *259*, 1409–1410.
44. Martin, E. F.; Hofmann, G. E. Heat-Shock Proteins, Molecular Chaperones, and the Stress Response: Evolutionary and Ecological Physiology. *Annu. Rev. Physiol.* **1999**, *61*, 243–282.
45. Gupta, S. C.; Sharma, A.; Mishra, M.; Mishra, R. K.; Chowdhuri, D. K. Heat Shock Proteins in Toxicology: How Close and How Far? *Life Sci.* **2010**, *86*, 377–384.
46. Madamanchi, N. R.; Li, S.; Patterson, C.; Runge, M. S. Reactive Oxygen Species Regulate Heat-Shock Protein 70 *via* the Jak/Stat Pathway. *Arterioscler., Thromb., Vasc. Biol.* **2001**, *21*, 321–326.
47. Zang, L.-Y.; Cosma, G.; Gardner, H.; Vallyathan, V. Scavenging of Reactive Oxygen Species by Melatonin. *Biochim. Biophys. Acta* **1998**, *1425*, 469–477.
48. Kadiiska, M. B.; Hanna, P. M.; Hernandez, L.; Mason, R. P. *In Vivo* Evidence of Hydroxyl Radical Formation after Acute Copper and Ascorbic Acid Intake: Electron Spin Resonance Spin-Trapping Investigation. *Mol. Pharmacol.* **1992**, *42*, 723–729.
49. Huang, X.; Zhuang, J.; Teng, X.; Li, L.; Chen, D.; Yan, X.; Tang, F. The Promotion of Human Malignant Melanoma Growth by Mesoporous Silica Nanoparticles through Decreased Reactive Oxygen Species. *Biomaterials* **2010**, *31*, 6142–6153.
50. Cross, J. B.; Currier, R. P.; Torraco, D. J.; Vanderberg, L. A.; Wagner, G. L.; Gladen, P. D. Killing of Bacillus Spores by Aqueous Dissolved Oxygen, Ascorbic Acid, and Copper Ions. *Appl. Environ. Microbiol.* **2003**, *69*, 2245–2252.
51. Gomes, A.; Fernandes, E.; Lima, J. L. F. C. Fluorescence Probes Used for Detection of Reactive Oxygen Species. *J. Biochem. Biophys. Methods* **2005**, *65*, 45–80.
52. Simon, H. U.; Haj-Yehia, A.; Levi-Schaffer, F. Role of Reactive Oxygen Species (Ros) in Apoptosis Induction. *Apoptosis* **2000**, *5*, 415–418.
53. Singh, N.; Manshian, B.; Jenkins, G. J. S.; Griffiths, S. M.; Williams, P. M.; Maffeis, T. G. G.; Wright, C. J.; Doak, S. H. Nanogenotoxicology: The DNA Damaging Potential of Engineered Nanomaterials. *Biomaterials* **2009**, *30*, 3891–3914.
54. Guo, W.-j.; Ye, S.-s.; Cao, N.; Huang, J.; Gao, J.; Chen, Q.-y. Ros-Mediated Autophagy Was Involved in Cancer Cell Death Induced by Novel Copper(II) Complex. *Exp. Toxicol. Pathol.* **2010**, *62*, 577–582.
55. Murakami, T.; Nakatsuji, H.; Inada, M.; Matoba, Y.; Umeyama, T.; Tsujimoto, M.; Isoda, S.; Hashida, M.; Imahori, H. Photodynamic and Photothermal Effects of Semiconducting and Metallic-Enriched Single-Walled Carbon Nanotubes. *J. Am. Chem. Soc.* **2012**, *134*, 17862–17865.
56. Chen, Q.; Chen, H.; Shapiro, H.; Hetzel, F. W. Sequencing of Combined Hyperthermia and Photodynamic Therapy. *Radiat. Res.* **1996**, *146*, 293–297.

57. Gottfried, V.; Kimel, S. Temperature Effects on Photosensitized Processes. *J. Photochem. Photobiol., B* **1991**, *8*, 419–430.
58. Huang, X.-L.; Zhang, B.; Ren, L.; Ye, S.-F.; Sun, L.-P.; Zhang, Q.-Q.; Tan, M.-C.; Chow, G.-M. *In Vivo* Toxic Studies and Biodistribution of near Infrared Sensitive Au−Au_2S Nanoparticles as Potential Drug Delivery Carriers. *J. Mater. Sci. Mater. Med.* **2008**, *19*, 2581–2588.
59. Prinsze, C.; Dubbelman, T.; Vansteveninck, J. Potentiation of Thermal Inactivation of Glyceraldehyde-3-Phosphate Dehydrogenase by Photodynamic Treatment. A Possible Model for the Synergistic Interaction between Photodynamic Therapy and Hyperthermia. *Biochem. J.* **1991**, *276*, 357–362.
60. Zha, Z.; Wang, S.; Zhang, S.; Qu, E.; Ke, H.; Wang, J.; Dai, Z. Targeted Delivery of Cus Nanoparticles through Ultrasound Image-Guided Microbubble Destruction for Efficient Photothermal Therapy. *Nanoscale* **2013**, *5*, 3216–3219.